Non-covalent and covalent immobilization of Candida antarctica Lipase B on chemically modified multiwalled carbon nanotubes for a green acylation process in supercritical CO2

Mohamed Chafik Bourkaib, Yann Guiavarc'h, Isabelle Chevalot, Stéphane Delaunay, Jerome Gleize, Jaafar Ghanbaja, Fabrice Valsaque, Nawal Berrada, Alexandre Desforges, Brigitte Vigolo

Non-covalent and covalent immobilization of *Candida antarctica* Lipase B on chemically modified multiwalled carbon nanotubes for a green acylation process in supercritical CO₂

Mohamed Chafik Bourkaib[1], Yann Guiavarc'h[1], Isabelle Chevalot[1], Stéphane Delaunay[1] Jérôme Gleize[2], Jaafar Ghanbaja[3], Fabrice Valsaque[3], Nawal Berrada[3], Alexandre Desforges[3], Brigitte Vigolo[3]

[1]Laboratoire Réactions et Génie des Procédés, University of Lorraine, CNRS, F-54000 Nancy, France

[2]Laboratoire de Chimie Physique-Approche Multi-échelle de Milieux Complexes, University of Lorraine, F-57078, Metz, France

[3] Institut Jean Lamour, University of Lorraine, CNRS, F-54000 Nancy, France

Abstract

Candida antarctica B lipase (CAL-B) was immobilized on purified and functionalized multiwalled carbon nanotubes (MWCNTs). Both immobilization routes, physical adsorption and covalent bonding, were investigated. MWCNT functionalization by a non-aggressive oxidation by potassium permanganate led to an interesting balance between the hydrophilic and the hydrophobic areas of the MWCNT surface; the former being responsible of the good dispersion of MWCNTs in water and the latter having a favorable affinity with CAL-B. The enzyme loadings reached were significant: around 16 wt. % and 21 wt.% for non-covalent and covalent immobilization, respectively. The enzymatic activity was studied with the reaction of O-acylation of geraniol into geranyl acetate by CAL-B in supercritical CO_2. Even if a decay in synthesis of geranyl acetate was observed over cycling for both CAL-B@MWCNT catalysts, it was demonstrated that the regioselectivity of CAL-B was unchanged through immobilization on the MWCNT surface for both routes. Interestingly, it was shown that a fully green enzymatic process can be achieved with these prepared CAL-B@MWCNT biocatalyst. Such approach could be transferred to other support/enzyme systems for developing new eco-friendly synthesis processes.

1. Introduction

Environmental pollution is one of the greatest problems that the world is facing today. Chemical industry belongs to the main sectors that have started to use and currently continue to look for processes capable of reducing contaminant release. In the academic domain, development of greener chemical methods has focused a growing attention recently and remains

challenging. Enzymatic catalysis is an interesting route which is compatible with development of fully environmentally friendly processes. Nevertheless, as the enzymes are free, their activity is usually disappointing. Interestingly, improvement of enzymatic conversions can be achieved by immobilizing them onto a support material surface [1]. Selecting an appropriate substrate and inducing favorable enzyme/substrate interactions are both crucial to prepare effective biocatalysts. The immobilization technique has been explored with great success since the immobilized enzymes have shown improved thermal and pH stability and capacity of being reused [1,2]. Compared to high porosity macroscopic materials, nanomaterials having large surface-to-volume ratio and high accessible external surface could avoid diffusion limitation of the reactants to the enzyme sites. Carbon nanotubes (CNTs) are considered as ideal nanomaterials for enzyme immobilization since they mainly offer high external surface, with a cylindrical geometry favorable to a high immobilization level and they have also superior mechanical and conductive properties [3]. Furthermore, CNTs can be easily chemically functionalized by diverse functional groups which offer the potential to use this nanomaterial for both non-covalent [4] and covalent [5] immobilization. CNTs have been shown to increase stability of *Candida antarctica* B lipase (CAL-B) [6]. Physically immobilized *Burkholderia cepacia* lipase on chemically modified CNTs resulted in significant enhancement of enzyme activity [7]. Phenylalanine ammonia-lyase covalently immobilized on carboxylated CNTs showed improved properties in continuous flow [8].

Lipases such as CAL-B are a widely known as a useful family of enzymes since they are capable of transferring the acyl group in organic solvents [9], in solvent-free reaction [10,11] or in ionic liquid [12,13]. Few studies reported esterification by CAL-B immobilized on CNTs and for all of them, organic solvents were required for the catalytic synthesis. [4,14,15] More recently, the unique properties of supercritical fluids (scFs) which are also a kind of green solvents, have drawn the attention of chemists. *Candida rugosa* lipase (CRL) was able to synthesize *trans*-2-phenyl-1-

cyclohexanol with high enantioselectivity in glucopyranoside in supercritical CO_2 (scCO$_2$) [16]. CRL was shown to catalyze the regioselective acylation of methyl 6-O-trityl b-d-glucopyranoside in scCO$_2$ with a conversion rate as high as 91.4 % [17]. Conversions of 83 % and 98 % were observed for the synthesis of geranyl acetate catalyzed by CAL-B in scCO$_2$ [18]. Even if more investigation is needed to better understand the precise involved mechanisms between the scFs and the biocatalyst, it has been normally observed that the reaction selectivity was preserved and the reaction rate was increased in scFs compared to other solvents. Moreover, the straightforward product collection without any traces of solvent is another advantage of working in scFs [19].

In this work, for the first time, the combination of the advantages of using multiwalled CNTs (MWCNTs) as support and scCO$_2$ as solvent was proposed for the synthesis of geranyl acetate catalyzed by CAL-B. Geranyl acetate belongs to the family of monoterpene esters being of great interest in cosmetics, pharmaceutics and food industry for their properties of floral scents and antibacterial effects. CNTs were chemically modified to increase their affinity with water. Both physical adsorption and covalent immobilization by amino-acid coupling were investigated. Thanks to a set of complementary techniques, the preparation of the biocatalysts was fully controlled. Acylation reaction of lysine by CAL-B@MWCNT was also carried out to check any modification of reaction selectivity for both types of immobilization on CNTs. Enzymatic synthesis of geranyl acetate was performed both by non-covalent and covalent immobilization of CAL-B onto MWCNT surface in scCO$_2$. The conversion rate was discussed in light of the possible interactions involved in the investigated systems.

2. Material and methods

2.1. Sample preparation

Potassium permanganate (KMnO$_4$) and sodium sulfite (Na$_2$SO$_3$) were purchased from Alfa Aesar, sodium hydroxide (NaOH) from VWR, and nitric acid (HNO$_3$) 65 % was acquired from Honeywell Fluka. Sulfuric acid (H$_2$SO$_4$) 95-97 % and hydrochloric acid (HCl) 37 % were provided by Sigma Aldrich.

2.1.1 Functionalization of carbon nanotubes

The used MWCNT sample was provided by Nanocyl S.A (NC7000). It was synthesized by a Chemical Vapor Deposition (CVD) method by using iron or cobalt as catalysts deposited on an alumina substrate. The as-produced or raw MWCNTs referred to as rMWCNT contained catalytic residues. For the selective removal of the metal-based impurities, rMWCNT was submitted to a chlorine-based treatment [20] at 1000°C for 2 h. The purified MWCNTs were named pMWCNT. They were functionalized following a liquid phase method using an alkaline solution of KMnO$_4$ [21,22]. Typically, 100 mg of the purified MWCNT powder were added to 60 mL of KMnO$_4$ 0.2 M and 60 mL of NaOH 0.2 M in a round bottom flask equipped with a condenser and refluxed for 40 min. After cooling down 3 g of Na$_2$SO$_3$ was added to reduce KMnO$_4$ in 35 mL of H$_2$SO$_4$ 1 M. Then, the powder was washed with HCl 4 N and with water several times until neutral pH. And the sample was dried overnight at 50 °C. The functionalized MWCNTs were referred to as fMWCNT.

2.1.2 Immobilization of CAL-B on the functionalized CNTs

For immobilization, an aqueous dispersion of 0.1 wt.% of fMWCNT was prepared using an ultrasonic probe Vibra cell 75042 during 15 min with a power of 125 W with a pulse mode 2 sec-ON/1 sec-OFF. The quality of the dispersion was verified by optical microscopy. The desired amount of CAL-B was added to set the CAL-B / fMWCNT weight ratio to 30 %.

For the non-covalent route (ncCAL-B@MWCNT), the mixture CAL-B and fMWCNT was stirred during the chosen duration in the 30 min – 3 h range. A fixed volume of the mixture was

5

taken at regular intervals at every 30 min of immobilization and filtrates on a PTFE membrane. The optimized immobilization duration was determined by two methods:

i) UV-Vis spectroscopy (by using a spectrometer Varian Cary 3E) by measuring the concentration of the non-adsorbed CAL-B in the filtrate for each sampling: by using a calibration curve with solutions of BSA (Bovine Serum Albumine) at known concentrations, the CAL-B assay was performed using a commercial Bicinchoninic Acid Assay (BCA) protein measurement kit. It contained a complexing agent which made it possible to reveal the presence of enzymes by a coloration in the visible spectral domain at 562 nm.

ii) TGA under He (see also below): after filtration, the solid CAL-B@MWCNT was dried and transferred into the TGA chamber. It was heated under helium (following the conditions given in section 2.2). MWCNTs were untouched under inert gas in the used temperature range (RT-900°C) while the functional groups and the enzymes were gasified. Subtracting the weight loss of the CAL-B@MWCNT to that of the fMWCNT was used to determine the weight corresponding to the amount of adsorbed enzymes [23].

The used covalent immobilization method was based on an amino-acid coupling. In a typical experiment, 300 mg of fMWCNT were dispersed in 600 mL of deionized water (DIW) and the pH was adjusted to 8 with NaOH. 4.8 g of 1-éthyl-3-(3-diméthylaminopropyl)carbodiimide (EDC), 4.8 g of (N-Hydroxysuccinimide) NHS and 100 mg of enzymes were added to the fMWCNT dispersion. The reaction was conducted at room temperature under stirring for 48 h. The prepared CAL-B covalently immobilized on MWCNTs (cCAL-B@MWCNT) were washed 3 times with DIW on a vacuum filtration set-up and dried by freeze-drying.

2.1.3 Activity assays of the prepared CAL-B@MWCNT

2.1.3.1 Chemicals and enzyme

Lysine and lauric acid were purchased from Sigma-Aldrich (Saint Quentin Fallavier, France) and 2-Methyl-2-butanol (M2B2) from Carlo Erba (France). The free lipase B of *Candida antarctica* (CAL-B) was kindly provided by Novozymes. Novozym 435® (CAL-B immobilized on an acrylic resin) with propyl laurate synthesis activity of 7000 PLU g−1 and protein grade of 1–10% was purchased from Novo Nordisk A/S (Bagsværd, Denmark).

2.1.3.2 Geranyl acetate synthesis

Geranyl acetate enzymatic synthesis with CAL-B@MWCNT was conducted through a packed bed reactor (PBR) by using a continuous automated high-pressure supercritical fluid equipment (SFC-CO$_2$) from JASCO (Tokyo, Japan) (Fig. 1). This equipment consisted in a CO$_2$ pump (Pu-2080- CO$_2$ Plus unit, JASCO, Japan) and a semi-micro HPLC pump for the two reaction substrates mixed together (Pu-2085 Plus unit, JASCO, Japan). The liquid CO$_2$ pump was equipped with an internal Peltier cooling system for cooling at - 4°C. In order to be sure that all CO$_2$ coming from the CO$_2$ bottle was in the liquid form, before pumping by the CO$_2$ pump, an additional cooling of CO$_2$ at -4°C was performed with a Lauda RM6 cryostat (Lauda-Königshofen, Germany). The pressure was controlled with an automated back-pressure regulator (BP-2085 Plus unit, JASCO, Japan) at a precision of ± 0.2 MPa of the setting value. This back pressure regulator (BPR) is based on the use of a CO$_2$ flow-switching valve (FSV) mechanism that enables stable system pressure control together with efficient collection of the SFE extract in a glass tube. Because CO$_2$ decompression is highly endothermic (Joule-Thomson effect), especially when using "high" CO$_2$ mass flow, and can generate CO$_2$ dry ice at the exit of the BPR, the latter was equipped with an internal Peltier heating system maintained at 60°C in order to avoid CO$_2$ solidification during decompression. A 30 mm length x 4.6 mm diameter Sulzer SMX™ stainless steel static mixer (Winterhur, Switzerland) was used for mixing scCO$_2$ and substrates before their entrance in the packed bed reactor (PBR). This PBR consisted of a 1/4 inch (6.35/4.6 mm external/internal) diameter * 65 mm length stainless steel tubing section

connected to 1/16 inch tubing with Swagelok VCR adaptors (Solon, Ohio, USA) equipped with stainless steel sintered pieces placed on both extremities of the reactors. Static mixer, PBR and tubing were placed in a Thermo Scientific HERAEUS 200L ventilated oven (Dreieich, Germany) for temperature regulation with a precision of ± 0.15 °C of the set $scCO_2$ temperature value. Figure 1 shows the schematic flow diagram of the extraction equipment. For each reaction run, the PBR was packed with CAL-B@MWCNT adjusted to a water activity of about 0.2. A constant flow rate of 40 μL/min of an equimolar freshly prepared mixture of geraniol and acetic acid as substrates was systematically mixed to a liquid CO_2 at -4 °C pumped at constant flow rate of 3 mL/min and pressure of 200 bars. After heating to 55 °C, the CO_2 became supercritical and expanded in such a way that the volume flow-rate became 3.94 mL/min and its corresponding residence time in the reactor was about 6 seconds. Substrates concentration in liquid CO_2 was 57 mM, which corresponded to 43.4 mM in $scCO_2$. Products (geranyl acetate and some traces of water) and unreacted substrates (geraniol and acetic acid) were collected in 60 mL amber vials at the exit of the back pressure regulator (BPR). For sample collection at atmospheric pressure all along the reaction, and as described in Bourkaib *et al.* a home-made CO_2 flow breaker was used for breaking CO_2 flow while allowing desolubilized products and unreacted substrates to flow in a liquid form along the internal walls of the flow breaker [18]. This flow breaker system was placed just above, and not inside the collecting tube, so that CO_2 can be easily eliminated in the atmosphere. At the end of each reaction run the system was purged from the residual $scCO_2$. The PBR was emptied, disassembled, and its elements were thoroughly washed with distilled water and acetone before drying. Sonication in water was used for the cleaning of sintered stainless-steel filters and static mixer.
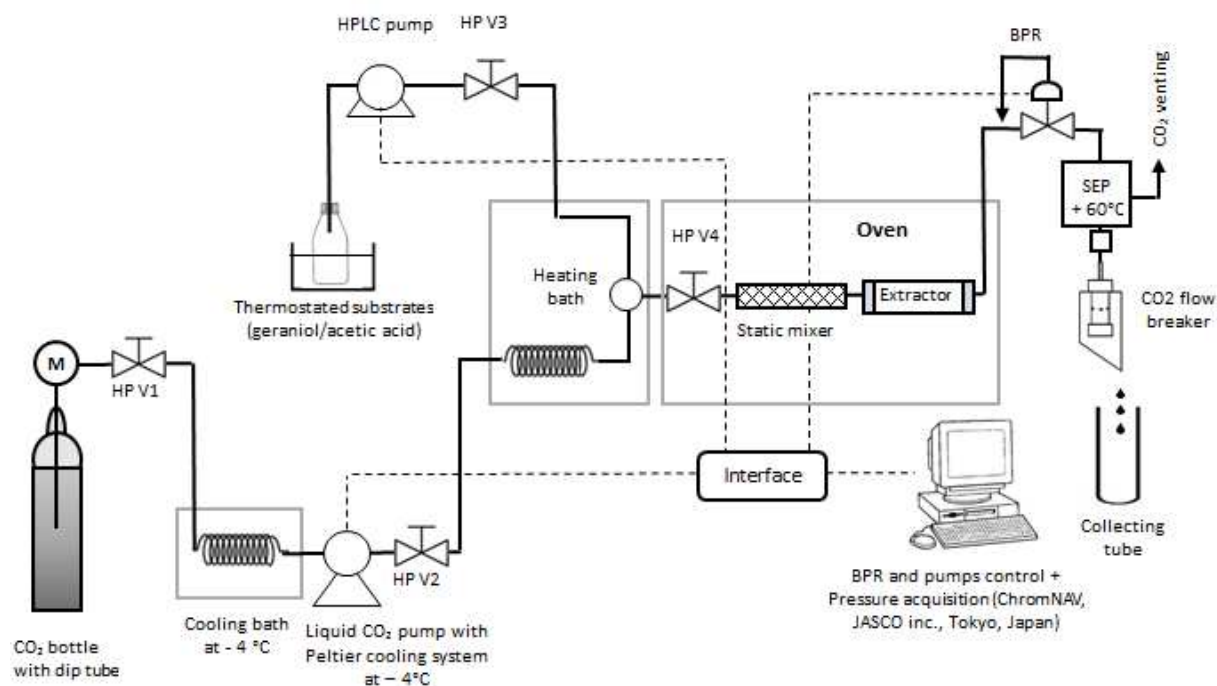
Figure 1 Schematic view of the supercritical CO_2 equipment. M: manometer, HP V1 to HP V4: high pressure manual valves, BPR: Back Pressure Regulator, SEP: Separator heated at 60°C with a Peltier system. Solid black lines represent tubing for CO_2 and liquid substrates. Dashed lines represent BPR and pumps control from ChromNAV software.

2.1.3.3 Lauroyl-lysine synthesis

The synthesis of lauroyl-lysine was carried out with L-lysine (0.12 M) and Lauric acid (0.24 M) in 2 mL of 2-methyl-2-butanol previously dehydrated on 4 Å molecular sieves. The acylation reaction was performed in an agitated parallel system (Carousel 12 Plus Reaction Station™, Radleys) initiated by the addition of CAL-B immobilized on acrylic resin, or functionalized MWCNTs by physi- or chemisorption. The quantity of the used supported enzymes was adjusted to add 1 mg of protein in the reaction medium depending on the immobilization yield. The reaction medium was stirred at 250 rpm at 55 °C. The samples were

withdrawn over time, diluted with methanol/water (50/50, v/v) to stop the enzyme activity, and then, stored at 4°C before HPLC–MS^2 analysis. Each reaction was done in duplicate.

The synthesis of lauroyl-lysine was followed as described by Dettori *et al.* [24]. A HPLC–MS^2 system was used consisting in a binary delivery pump connected to a photodiode array detector (PDA) and a LTQ ion trap as mass analyzer (Linear Trap Quadrupole) equipped with an atmospheric pressure ionization interface operating in positive electrospray mode (ThermoFisher Scientific, San Jose, CA, USA). A C18 column (150 mm×2.1 mm, 5 μm porosity– Grace/Alltech, Darmstadt, Germany) equipped with a C18 pre-column (7.5mm×2.1 mm, 5 μm porosity– Grace/Alltech Darmstadt, Germany) at 25 °C was used for the chromatographic separation. Mobile phases corresponded to methanol/water/ TFA (80:20:0.1, v/v/v) for the phase A and methanol/TFA (100:0.1, v/v) for the phase B. The elution was carried out using a linear gradient from 0 % to 100 % of B for 5 min and then an isocratic step at 100 % of B for 10 min, at a flow rate of 0.2 mL min^{-1}. These conditions allowed the separation of α-lauroyl lysine and ε-lauroyl lysine with 9.39 min and 10.0 min retention times, respectively. Mass spectrometric conditions consisted in spray voltage at + 4.5 kV with capillary temperature at 250 °C and capillary voltage at 48 V; tube lens, split lens and front lens voltages were set at 120 V, −34 V and −4.25 V, respectively. Full scan MS spectra were performed from m/z 100 to 1000 and additional MS^2 scans were done in order to verify the enzyme selectivity thanks to structural information based on daughter ions elucidation. Raw data were processed using Xcalibur software (version 2.1 Thermo Scientific).

2.2. Techniques used for nanomaterial characterization

The used optical microscope was an Olympus TH4-200 BXS1. The solution was simply dropped on a microscope slide and covered by a cover glass. Observations were done with an X10 objective.

TEM and HRTEM observations were done by means of a JEOL ARM 200F cold FEG apparatus (operating voltage of 80 kV). A nitrogen liquid-cooling (-175 °C) sample holder was used to image the enzymes. The TEM grids (holey carbon grid, 200 mesh size) were prepared by depositing a drop of a suspension of the sample dispersed by gentle sonication in ethanol. At least 30 images from the observations of many zones on the grid were analyzed; the shown TEM images are those representative of the general aspect of the observed samples.

TGA was carried out with a Setaram Setsys evolution 1750 Thermal Gravimetric Analyser. Temperature was increased from room temperature to 900°C at 5 °C/min under dry air or helium (20 mL/min). For mass spectrometry (MS) investigation, a Pfeiffer GSD 301C Vacuum OmniStar mass spectrometer coupled with the TGA apparatus was used.

Raman spectroscopy characterization was performed using a LabRAM HR 800 micro-Raman spectrometer (incident wavelength 632.8 nm, power 0.25 mW/μm^2). To guarantee reproducibility, at least three spectra were recorded on different areas for the same sample. For Raman frequency calibration, a silicon wafer was used as reference. For data analysis, after subtracting a baseline, the I_D/I_G intensity ratio was calculated from the maximum height of the D and the G band for each spectrum.

Adsorption volumetry was performed using krypton at 77.3 K. Before analysis, the MWCNT samples were outgassed under a vacuum of $4\ 10^{-5}$ Pa at 180 °C for at least 5 days. The isotherms were normalized by the amount of carbon content (from TGA) in the samples. The specific surface area of the samples was determined by using the well-known Brunauer-Emmett-Teller (BET) model.

3. Results and discussion

3.1. Maximizing the accessible surface of the MWCNTs for CAL-B immobilization

Controlling MWCNT characteristics is essential in order to optimally benefit of the surface they can offer during the subsequent immobilization of the enzymes. Ideally, an "all-carbon" material is desired to avoid competing and non-controlled reactions and to control the quality and quantity of the substrate. The purification of MWCNTs was performed by a one-pot gas phase treatment. In the raw sample, there was no carbonaceous impurity and the metallic impurities were present under several forms: cobalt and/or iron oxides and/or carbides and alumina. The used purification method has the advantage to remove all these noncarbon residues with the same treatment since chlorine is expected to favorably react with all these metals [20]. The quantitative evaluation of the metal-based impurity content was conducted by TGA (Fig. 2).
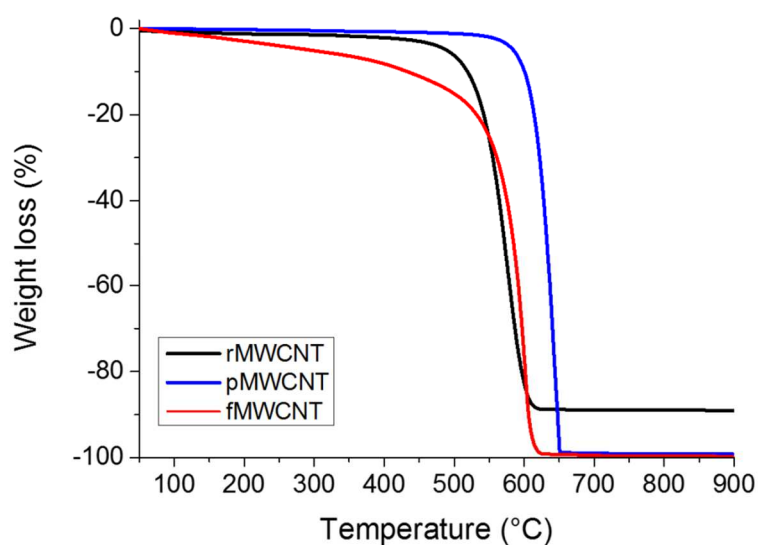
Figure 2 Thermograms of the raw (black), purified (blue) and functionalized MWCNTs (red).

The difference between the thermogram of the raw (rMWCNT) and that of the purified MWCNTs (pMWCNT) was significant. The main weight loss came from combustion of MWCNTs occurring around 570 °C and 630 °C for rMWCNT and pMWCNT, respectively.

Furthermore, the content of metal-based impurities (remaining amount after MWCNT combustion) was about 11.1 wt.% of the initial mass for the raw MWCNTs and reached zero after purification. This attested to the high efficiency of the applied purification treatment for this MWCNT sample. In addition, the observed upshift (+60 °C) of the combustion temperature after removal of the metal-based impurities is usually explained by the elimination of metallic particles. These latter have been shown to catalyze the combustion reaction of MWCNTs, which leads to their lower oxidation resistance [25].

After functionalization, it can be noted that there was no plateau for temperatures below 500 °C and the combustion appeared at lower temperature (about 585 °C). Such lower oxidation resistance may be due to the functional groups or defects that had been introduced to the CNT walls through the functionalization procedure.

Figure 3 shows TEM images of the MWCNTs at their raw, purified and functionalized state. For all samples, the MWCNTs appeared as nanowires with the well visible inner channels especially at high magnification images (b, c, d). The outer diameter of the tubes was around 10-15 nm and the number of their walls could vary from 3 to 15. Their inner channel size often reached 10 nm. No carbonaceous species other than CNTs were observed in the samples. The metal-based impurities could be observed time to time as dark particles (see insert Fig. 3a). Except for the absence of the metallic impurities, the purified MWCNTs showed no significant changes compared to starting sample (Figs. 3c and 3d). By contrast, after functionalization, the walls of fMWCNT appeared damaged. Raman spectroscopy is widely used to evidence covalent functionalization of CNTs [26]. The D band (around 1350 cm^{-1}) reflects the presence of structural defects in CNT walls and the G band (around 1600 cm^{-1}) is characteristic of C=C double bonds from the sp^2 network. Increase in intensity of the D band with respect to that of the G band (I_D/I_G), is considered as the signature of defect introduction in CNT structure due to

grafting of functional groups. In Figure 4, the Raman intensity was normalized to that of the G band, in that respect, the D band intensity can be visually compared.
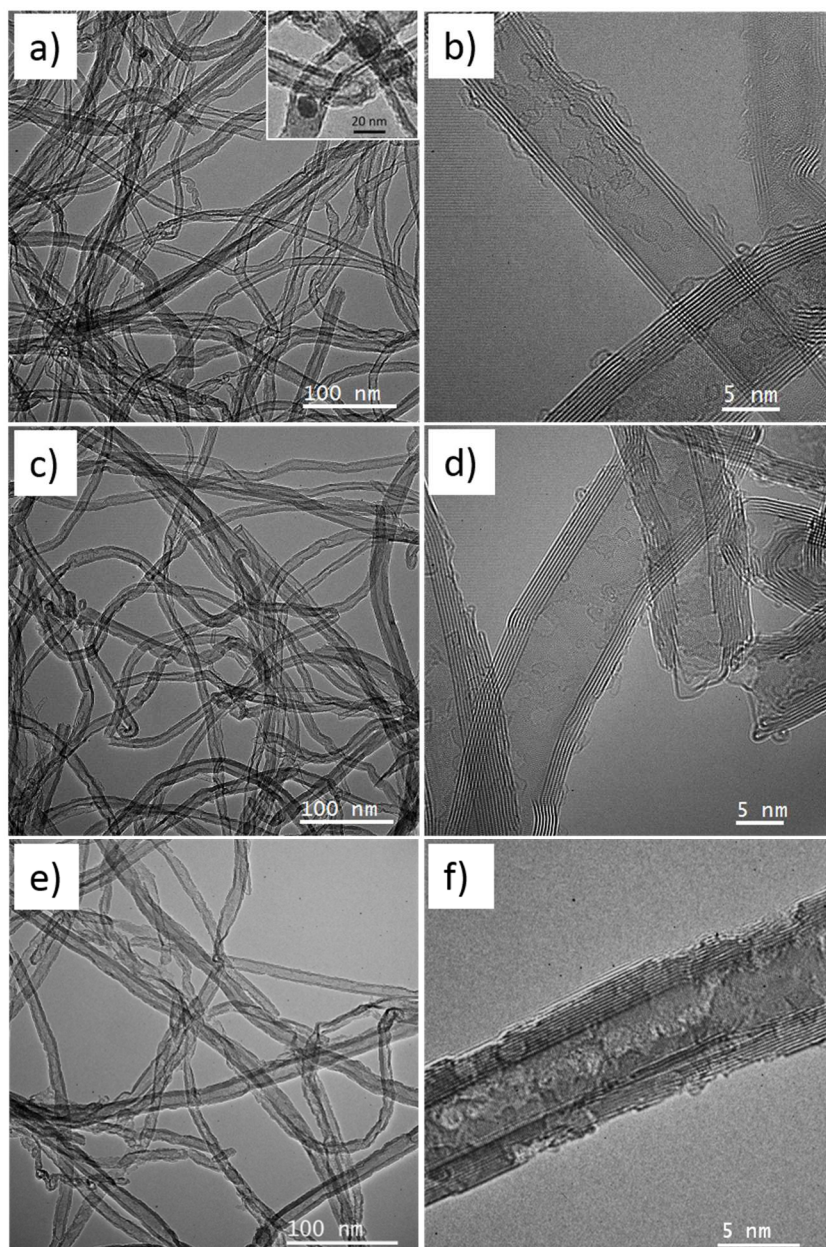
Figure 3 Typical bright field TEM images of (a and b) the raw (rMWCNT), (c and d) the purified (pMWCNT) and (e and f) the functionalized MWCNTs (fMWCNT) with low magnification (a, c, e) and high magnification (b, d, f).

I_D/I_G was around 1.8 and 1.6 for rMWCNT and pMWCNT, respectively. The intensity of the D band was slightly decreased after purification meaning that the purification treatment did not damage the MWCNTs. After functionalization, the D band was much more pronounced (I_D/I_G was about 2.2 for fMWCNT) in agreement with an efficient functionalization by the applied chemical method.
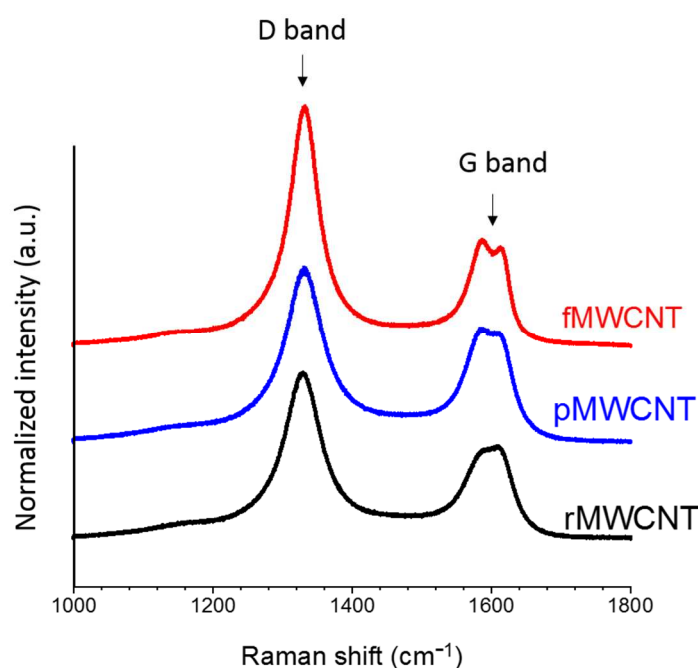

Figure 4 Raman spectra of the raw (rMWCNT), the purified (pMWCNT) and the functionalized MWCNTs (fMWCNT).

As already mentioned, carbon nanotubes are interesting support for enzyme immobilization because they offer high external surface which is potentially rapidly accessible compared to porous materials such silica, other porous oxides or synthetic polymers [1]. In this work, for surface property investigation, it was chosen to use krypton as adsorbate; being a rare gas, krypton adsorption phenomenon on the CNT surface will only be physical. Figure 5 shows the

15

adsorption isotherms for rMWCNT, pMWCNT and fMWCNT. The isotherms of the raw and purified MWCNTs were quite similar. In agreement with TEM and Raman spectroscopy results, adsorption study revealed that the applied purification treatment left the properties of the nanotube surface unchanged. The isotherms for these two samples showed some steps (type VI form the IUPAC classification). Each step corresponded to the formation of a Kr monolayer and these steps were characteristic of the adsorption on a fraction of uniform, homogeneous surface in agreement with the poorly-defected structure of rMWCNT and pMWCNT [27,28]. The isotherm of the functionalized MWCNTs showed a very different shape with i) disappearance of the steps indicating that the adsorption process occurred on less homogeneous surfaces and ii) larger gas quantities adsorbed, which was probably due to the damaging of the MWCNT walls by functionalization.
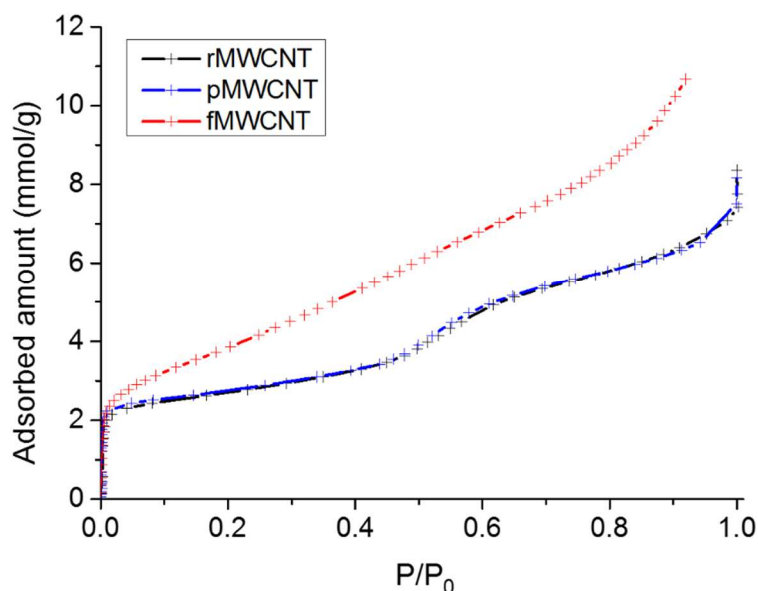
Figure 5 Krypton adsorption isotherms on rMWCNT, pMWCNT and fMWCNT at 77.3 K. P/P_0: normalized krypton equilibrium pressure relatively to its saturation vapor pressure, 227 Pa.

Using the well-known Brunauer-Emmett-Teller (BET) model, the specific surface areas extracted from the adsorbed amounts plotted in Figure 5 were quite similar for the raw and purified samples (201 m²/g for rMWCNT and 207 m²/g for pMWCNT). This was consistent with the preservation of the nanotube surface properties during the purification treatment. Regarding the functionalized sample, the BET model gave a specific surface area about 40 % greater (287 m²/g for fMWCNT). The observed increase in surface after functionalization is in agreement with previous works.[29,30] Functionalization is indeed able to open tube ends and generate defects on the sidewall of nanotubes, which gives access into the cavity of MWCNTs and increases that way their surface area.[29–31]

The prepared functionalized MWCNTs showed interesting properties for their further use to immobilize CAL-B since their functionalization resulted in an increase of the accessible surface and the evidenced efficiency of the functionalization treatment was expected to increase their affinity with the used water medium for immobilization.

3.2. Immobilization of CAL-B on the chemically modified MWCNTs

3.2.1. Optimization of the functionalized dispersion quality

CAL-B was immobilized in water at pH 10 (by NaOH addition) instead of in a Tris buffer solution because of the strong and rapid aggregation of fMWCNT observed in the buffer solution while the functionalized MWCNTs showed a quite good dispersion quality in alkaline water (Fig. 6). At pH 10, the carboxylic groups expected to be grafted to the MWCNT surface (see Supporting Information, Fig. S1) were expected to be deprotonated leading to electrostatic repulsive forces probably responsible for the good dispersion quality in alkaline water. The re-aggregation within

the buffer solution might be due to an ionic effect screening due to the high ionic strength in this medium.
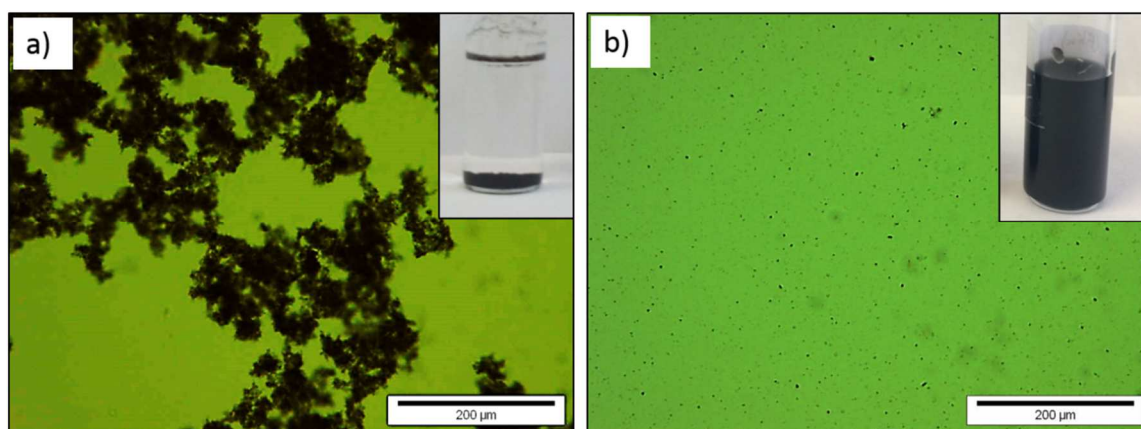
Figure 6 Optical microscope images of fMWCNT in Tris buffer solution (a) and in alkaline water (b). The visual aspect of each corresponding solution is visible in the insert at the top right corner of the corresponding image.

3.2.2. Immobilization kinetic

The kinetic for the non-covalent immobilization of CaL-B was studied in alkaline water by TGA (Fig. 7) and by UV-Vis (see Supporting Information, Fig. S2). Although based on a really different principle, the results obtained by these two techniques were in good agreement. For the following study, TGA was preferably investigated. The maximum immobilization level was reached after 1-2 h around 15 wt.%. For the preparation of ncCAL-B@fMWCNT catalyst, the immobilization time was fixed at 2 h.
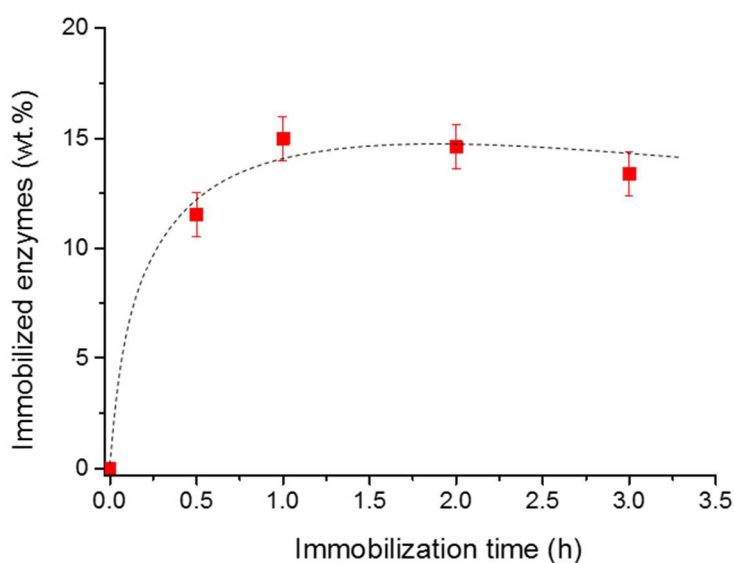
Figure 7 Immobilization kinetic for non-covalent adsorption of CAL-B on fMWCNT from TGA analysis.
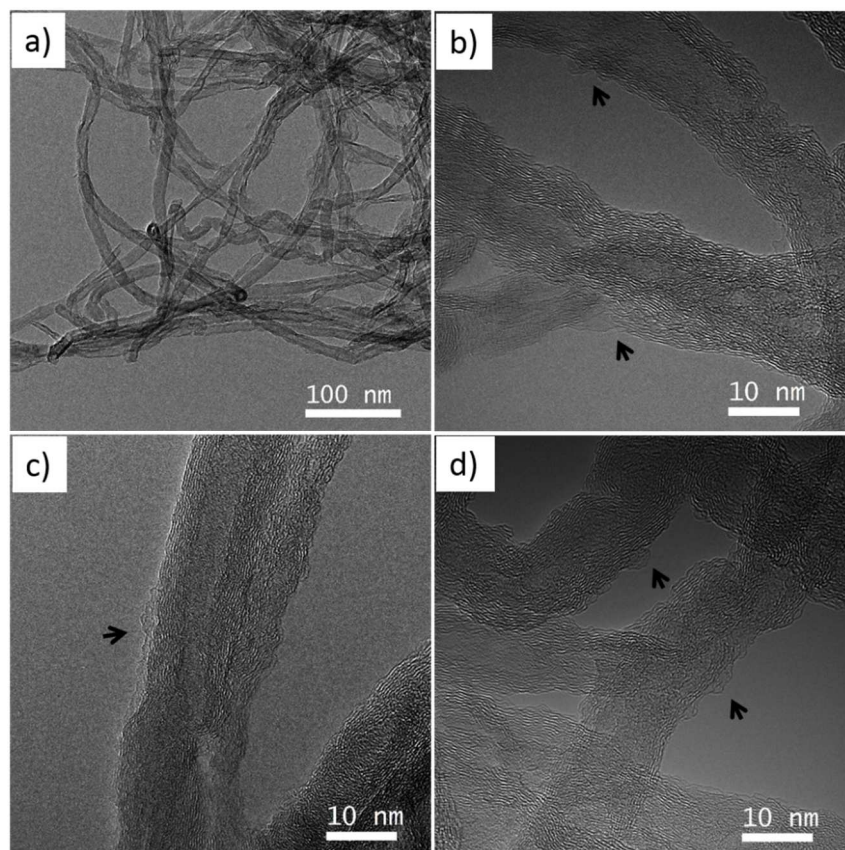
3.2.3. Non-covalent immobilization and covalent immobilization

The weight loss of the prepared non-covalent CAL-B@fMWCNT from TGA is shown in Figure 8a. An additional loss (+ 16 %, cf. Table 1), compared to that of fMWCNT was observed on the TGA curve of ncCAL-B@fMWCNT. By MS, phenyl group features can be used as the signature of the presence of enzymes in the material. The MS features showed that typically m/z 51 was only visible after immobilization (Fig. 8b). For sake of clarity, only this fragment was shown but the others belonging to phenyl groups (see Supporting Information, Fig. S3) were also well active after immobilization and not before.
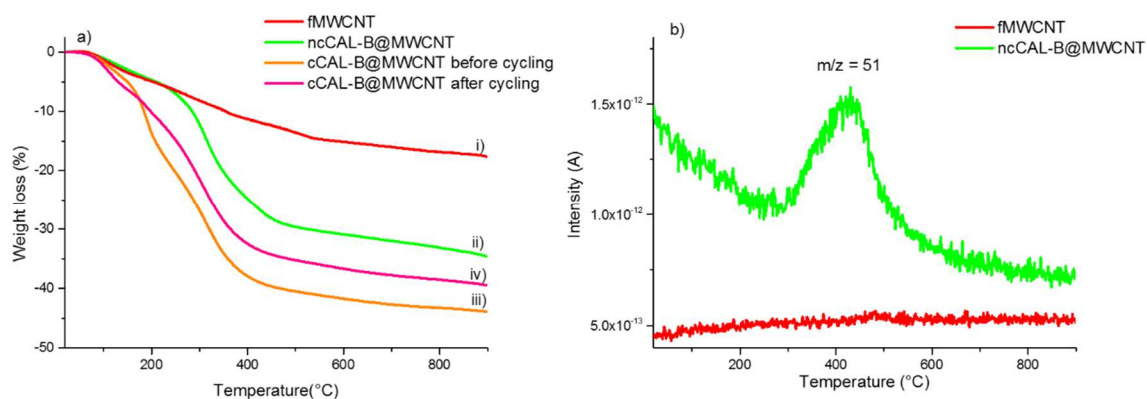
Figure 8 TGA-MS results; (a) TGA of fMWCNT (i), ncCAL-B@fMWCNT (ii), cCAL-B@MWCNT before cycling (iii) and cCAL-B@MWCNT after cycling (iv) and b) m/z 51 of fMWCNT and ncCAL-B@MWCNT.

Figure 9 shows TEM images of CAL-B covalently immobilized on the MWCNTs. At low magnification (Figure 9a), as expected, the aspect of the MWCNTs was similar to that of the functionalized MWCNTs. At higher magnification (Figs. 9b, 9c and 9d), an amorphous deposit assigned to the enzymes could be observed on the external surface of the MWCNT walls. These latter appeared differently than those of the functionalized MWCNTs (Fig. 3f) in agreement with the presence of numerous CAL-B enzymes (26 wt.%, Table 1) surrounding the MWCNTs modifying the wall appearance in the images.

Figure 9 Typical bright field TEM images of cCAL-B@MWCNT (before cycling) at (a) low magnification and (b, c, d) high magnification. Arrows help to localize the enzymes on the MWCNT surface.

A completely selective covalent immobilization is never easy to achieve since the enzymes surrounding the substrate cannot be forbidden to physically adsorb as well. It is certainly the case for fMWCNT which showed a good ability for non-covalent CAL-B immobilization (16 wt.%, Table 1). This is the reason why enzyme quantification for cCAL-B@MWCNT was performed just after the covalent immobilization process and after several reaction cycles (after activity stabilization, cf. the following section) after leaching of the non-covalently adsorbed CAL-B (Fig. 8). This approach allowed to selectively determine the covalent immobilization level (Table 1).

Table 1 Loading of CAL-B immobilized on the functionalized MWCNTs determined for CAL-B non-covalently immobilized on the functionalized MWCNTs (ncCAL-B@MWCNT) and CAL-B covalently immobilized of the functionalized MWCNTs (cCAL-B@MWCNT) before and after cycling.

Sample/Catalyst	fMWCNT	ncCAL-B@ MWCNT	cCAL-B@ MWCNT before cycling	cCAL-B@ MWCNT after cycling
Weight loss by TGA (%)	17	33	38	43
CAL-B loading (wt.%)	-	16	26	21

From the mass loss recorded for fMWCNT and by hypothesizing that the grafting groups were mainly carboxyl acids [21], the functionalization level could be estimated from the following relation (1) [32]:

$$n = \frac{M_{COOH}}{M_C}\left(\frac{100}{WL} - 1\right) \qquad (1)$$

Where M_{COOH} and M_C are the molar weights of a carboxyl acid group and a carbon atom, respectively; and WL, the weight assigned to the functional group loss from TGA, *i.e.* 17 % (Fig. 8 a and Table 1). n determined from (1) was about 18. That means that the used functionalized MWCNTs for CAL-B immobilization bear 1 functional groups every 18 carbon atoms or one functional group was grafted every 3 C_6-rings, in average. Furthermore, it is known that the applied oxidative attack leads to preferential grafting at the defects and at the extremities of the MWCNTs which are much more reactive sites than the sp^2 carbon atoms of the MWCNT skeleton [33,34]. This

is the reason why the functional groups were certainly not homogeneously disseminated on the MWCNT surface leaving rather large areas untouched, these latter remaining that way more hydrophobic while the functionalized areas (hydrophilic) were responsible for the facile dispersion of the MWCNTs in water. Physical adsorption of CAL-B enzymes possessing as well hydrophobic parts reached 16 % in weight of protein loading which was comparable of other works [4,23]. The used amino-acid coupling for covalent immobilization significantly increased the protein loading even after elimination of the non-covalently adsorbed (5 %) since it remained as high as 21 % after cycling.

3.3. Geranyl acetate synthesis in scCO$_2$

Geranyl acetate synthesis was performed with both ncCAL-B@MWCNT and cCAL-B@MWCNT under scCO$_2$ by using the set-up shown in Figure 1. For all experiments, the residence time in the PBR was as short as about 6 seconds. The conversion rate of geraniol to geranyl acetate by the prepared biocatalysts over cycling is shown in Figure 10. At cycle 1, significant conversions of 9.9 % and 6.9 % could be observed for ncCAL-B@MWCNT and cCAL-B@MWCNT, respectively. From cycle 1 to cycle 5, however, a significant decay in conversion was observed in both cases. This decay when using ncCAL-B@MWCNT could be due to very fast depressurization steps (200 to 1 bar in about 8 seconds) between each cycle that might lead to CAL-B leaching from the MWCNT surface. Besides, MWCNTs have a high mechanical and thermal resistance but low internal porosity compared to polymetacrylate-based polymers for example, which could also favor CAL-B leaching.
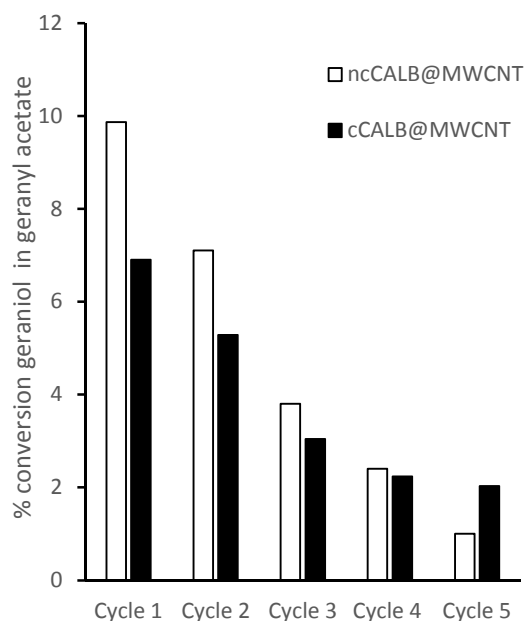
Figure 10 Conversion rate (%) of geraniol and acetate in geranyl acetate in $scCO_2$ using ncCAL-B@MWCNT (white bars) or cCAL-B@MWCNT (black bars). Experimental conditions: $scCO_2$ at 55°C and 200 bars, $scCO_2$ flow rate of 3.94 mL/min (3mL/min in liquid form), substrates concentrations of 43.4 mM in $scCO_2$, approx. residence time in the fully charged 1 mL PBR was only 6 seconds, 132 mg of ncCAL-B@MWCNT or cCAL-B@MWCNT in the reactor, 300 mg of Lipozyme 435 beads, 30 min per run.

Catalytic performances of the prepared biocatalysts (ncCAL-B@MWCNT and cCAL-B@MWCNT) were compared with those of a commercial lipase immobilized on polymeric meso-macroporous beads (Lipozyme 435) achieved under $scCO_2$ in the reactor using the same operating conditions [18]. In that former study, the reactor was filled with 300 mg of Lipozyme 435 beads (corresponding to 1 mL bulk volume) and 36 % conversion had been achieved without any change over 6 consecutive running cycles.

When focusing on the conversion rate achieved with cCAL-B@MWCNT, it could be observed that despite a decay in conversion, a plateau in conversion was reached starting from cycle 4. Moreover,

at cycle 5, conversion clearly turned in favor of cCAL-B@MWCNT (2 % against only 1% with ncCAL-B@MWCNT), thus showing the interest of using covalent binding with the prepared MWCNTs. Even if the activity observed for the present MWCNT-based catalysts remained to be improved by further investigations. Interestingly, it was demonstrated here that MWCNTs can be used as carriers for lipase and used for terpene ester production in $scCO_2$, which has never been demonstrated before.

To go further in the analysis of the conversion results for our MWCNT-based biocatalysts, the Turn Over Frequency (TOF) of CAL-B was determined, expressed in mole of geranyl acetate per mole of CAL-B per min for CAL-B immobilized non covalently or covalently on MWCNTs, before and after cycling (4 additional consecutive runs of 30 min each) (Table 2).

Table 2 TOF of CAL-B immobilized by covalent or physical adsorption on the functionalized MWCNT, before or after cycling (for covalent immobilization).

1 cm^3 bulk volume in the reactor	TOF (M geranyl acetate.M^{-1} CaL-B. min^{-1})
ncCAL-B@MWCNT before cycling	2.7
cCAL-B@MWCNT before cycling	11.5
cCAL-B@MWCNT after cycling	4.1

Before cycling ncCAL-B@MWCNT and cCAL-B@MWCNT showed a TOF of 2.7 and 11.5 moles of geranyl acetate.mole^{-1} of CAL-B.min^{-1}, respectively. After cycling, cCAL-B@MWCNT, showed a stabilized residual TOF of 4.1 moles of geranyl acetate.mole^{-1} of CAL-B.min^{-1}, while twice lower and non-stabilized TOF was achieved with non-covalent binding. When comparing these data with

data obtained previously by Bourkaib *et al.* [18] in similar operating conditions but using 300 mg of Lipozyme 435 beads (10.08 % w:w of CAL-B according to dos Santos *et al.*[35]), it was observed a significantly higher TOF of 62.7 moles of geranyl acetat.mole^{-1} of CAL-B.min^{-1}, expected for this commercial meso-macroporous catalyst. Furthermore, development of new biocatalysts using CNTs as support on which CAL-B was covalently or non-covalently immobilized has emerged over the past few years.

In addition, and despite the lower TOF achieved in this study with MWCNTs as carriers versus what was achieved by other authors such as Bourkaib *et al.* with commercial polymeric macroporous beads[18], it is of great importance to underline the specificity of the present process as compared to the ones observed from literature and also using MWCNTs as carriers. Indeed, when using continuous processing with a packed bed reactor, it was actually not required to perform cycling because reaction products and substrates and CO_2 are continuously removed from the reactor at the level of the back-pressure regulator-separator. Five consecutive 30 min catalytic cycles were performed with a depressurization step between each of them in order to proceed like in most studies where batch reactors are used (see Table S1). At cycle 5, only 10.1 % of unstabilized activity was retained in non-covalent immobilization (TOF of 2.05 min^{-1}) and 28.5 % in covalent immobilization (TOF of 4.1 min^{-1}). But if the reaction had been prolonged during several hours, the conversion would probably stay very close from the ones of cycle 1 (i.e. 9.9 % and 6.9 % in non-covalent and covalent immobilization, respectively). Corresponding TOF would probably have then be equal or very close to 11.5 min^{-1} when focusing on covalent immobilization (Table 2). When comparing these results with the ones achieved recently by Szelwicka *et al.*, who used CAL-B non-covalently immobilized on MWCNTs to esterify succinic acid with n-butanol in cyclohexane and in a batch reactor[14], it can be observed that a TOF of 10.9 min^{-1} was reached. Although substrates used for the esterification reaction are different, this result shows that the catalytic performance in

esterification of immobilized CAL-B in continuous reactor and with scCO$_2$ as a solvent was actually quite similar, the main difference being that CO$_2$ was used as a green solvent in a continuous process removing water continuously from the reactor.

Furthermore, it should be stressed, that according to Chrastil equation[36] the solubility of water in a supercritical CO$_2$ at 200 bar and 55°C is 2.32 mg/mL (see also Supporting Information) and that, even considering a full conversion of 57 mM substrates concentrations, it would generate only 1.026 mg of water per mL of supercritical CO$_2$ thus avoiding liquid water in the reactor and associated reverse hydrolysis reaction. This water solubilized in the CO$_2$ is continuously removed from the reactor all along each run, at the level of the back-pressure separator. This is precisely why, with the same reactor, Bourkaib *et al.* could reach 36% conversion in similar conditions but using the commercial Lipozyme 435.[18]

The TOF was however significantly higher (about 4 times) by using covalent binding as compared to non-covalent binding (Table 2). It can be supposed that the active site of CAL-B might be less accessible to substrates due to an unfavorable positioning for physical adsorption of CAL-B on the quite hydrophobic treated MWCNTs used here. Figure 11 shows a mapping of the surface of CAL-B with its hydrophobic and hydrophilic zones. It was designed from 1TCA PDB code and using PyMOL Molecular Graphics System (Schrodinger LLC, Portland, OR, USA). When using a simple adsorption on the used MWCNTs having hydrophobic domains, the active site of the CAL-B close to its hydrophobic zones will spontaneously position toward the surface of the MWCNTs thus potentially limiting accessibility of substrates to its catalytic triad. This scenario is consistent with the good affinity of proteins and lipases for hydrophobic carrier material reported in literature [37–40]. Conversely, when using covalent binding with NH$_2$ groups from lysine residues, it is very likely that the active site is more accessible to the substrates because, among the 9 lysine residues of CAL-B, none is very close from the active site entrance and 6 of them are clearly on the opposite side of the active site.

a)   b)


Active site cavity
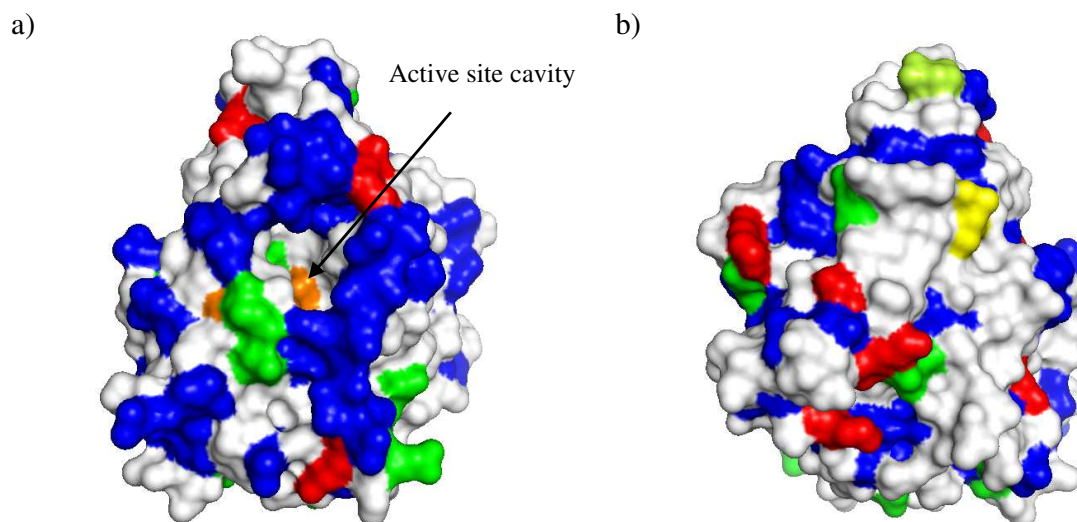
Figure 11 CAL-B surface with its hydrophobic and hydrophilic zones. Hydrophobic residues gly,

ala, val, leu, ileu, tyr, cys, met, phe are represented in blue; hydrophilic residues asp and glu are

represented in green; hydrophilic residue Lys (used for covalent binding) are represented in red;

catalytic triad of the active site (Ser 105, Asp 187, His 224) is in orange; N and C terminal residues

are shown in yellow and lemon yellow, respectively. a) active site and mainly hydrophobic side, b)

opposite and mainly hydrophilic side (180° rotation). These two figures were designed using

PyMOL Molecular Graphics System and 1TCA PDB code for CAL-B.

3.4. **Selectivity of supported enzymes on carbon nanotubes**

As the activity appeared to be affected by the immobilization method, it was also checked

whether it led to a modification of regio-selectivity. Several studies reported that enzyme

immobilization can lead to modification of the reaction selectivity depending on the

morphologies (average pore diameter, surface area, etc.) and nature of the supports [41]. For

instance, the regioselectivity of lipases can be modified by its immobilization on hydrophobic

supports: *Thermomyces lanuginosus* lipase adsorbed on C18 supports lost its 1,3

regioselectivity towards the hydrolysis of oils [42]. In the present study, the synthesis of lauroyl

lysine catalyzed by the two prepared MWCNT-based catalysts was investigated and compared with Novozym 435 as a reference. Acylation of lysine can lead to the synthesis of 3 different products including two monoacylated products in α or ε position and a diacylated product. A previous work showed that the synthesis of mono lauroyl-lysine mainly occurred by Novozym 435 catalysis with a regioselectivity towards the amine function in ε position and no diacylated molecule was synthesized [24].

The qualitative analyses of reaction medium for both supported enzymes systems on MWCNTs by TLC demonstrated the presence of spots corresponding to monoacylated lysine with a retention factor of 0.58 similar to that obtained for reaction with Novozym 435 (data not shown). The analysis of the synthesized products by HPLC-MS^2 confirmed the production of the monoacylated lauroyl-lysine with a mass peak of [M+H]$^+$ of 329. Furthermore, the fragmentation of this mass peak (Fig. 12) led to one major daughter ion ([M+H]$^+$ of 266) corresponding to [(lauroyl-K) – H$_2$O – COOH + H]$^+$, and some minor daughter ions ([M+H]$^+$ of 197; 283 and 293) corresponding to the specific mass spectrum profile of lysine acylated by lauric acid in ε position. Consequently, similar regioselectivity has been demonstrated for CAL-B of immobilized on MWCNTs and with Novozym 435.
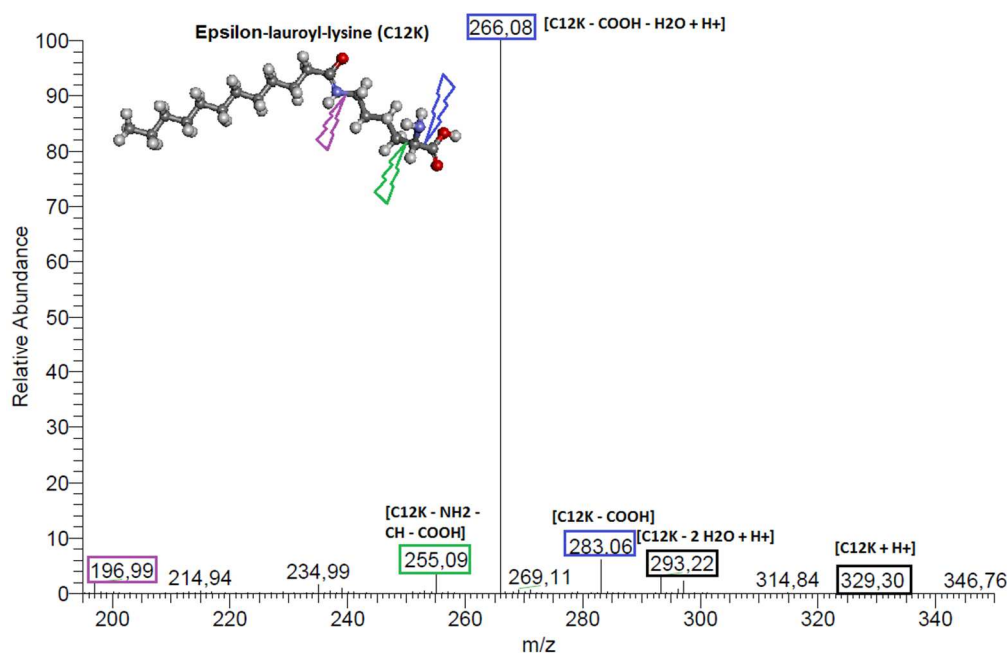
Figure 12 MS^2 spectrum of the peak corresponding to the monoacylated product ([M+H]$^+$ = 329) obtained by acylation of lysine with lauric acid catalyzed by CAL-B adsorbed on MWCNTs. Similar MS^2 spectrum was obtained for CAL-B immobilized by covalent bonds to MWCNT surface.

Conclusion

Synthesis of geranyl acetate by CAL-B immobilized on functionalized MWCNTs was investigated in supercritical CO_2 for the first time. Post-synthesis functionalization of purified MWCNTs by a relatively soft oxidant method has allowed to counterbalance the attractive van der Waals forces at the origin of the commonly observed CNT aggregation in water. The chemically modified MWCNTs also bear remaining hydrophobic zones which were evidenced as favorable adsorption sites in the case of the non-covalent route. The accessible surface could be advantageously improved leading to good CAL-B loadings for both non-covalent and covalent immobilization. The determined enzymatic activity for this fully green continuous process was in the same order of magnitude than that reported for CAL-B@CNT catalysts used

in conventional batch conditions in organic solvent. CAL-B regioselectivity of conversion was shown to be unchanged by using the prepared functionalized MWCNTs as support. Improvement of the conversion rate for new catalysts derived from the present work is in progress. The important finding of this work is that MWCNTs are promising support materials for enzymatic synthesis in supercritical CO_2, which could open a new field of investigations in biocatalysis.

Supplementary Information

Supplementary material related to this article can be found in the online version.

Acknowledgments

References

(1)   Zdarta, J.; Meyer, A. S.; Jesionowski, T.; Pinelo, M. A General Overview of Support Materials for Enzyme Immobilization: Characteristics, Properties, Practical Utility. *Catalysts* **2018**, *8* (2), 92. https://doi.org/10.3390/catal8020092.
(2)   Shuai, W.; Das, R. K.; Naghdi, M.; Brar, S. K.; Verma, M. A Review on the Important Aspects of Lipase Immobilization on Nanomaterials. *Biotechnol. Appl. Biochem.* **2017**, *64* (4), 496–508. https://doi.org/10.1002/bab.1515.

(3)   Feng, W.; Ji, P. Enzymes Immobilized on Carbon Nanotubes. *Biotechnol. Adv.* **2011**, *29* (6), 889–895. https://doi.org/10.1016/j.biotechadv.2011.07.007.

(4)   Pavlidis, I. V.; Tsoufis, T.; Enotiadis, A.; Gournis, D.; Stamatis, H. Functionalized Multi-Wall Carbon Nanotubes for Lipase Immobilization. *Adv. Eng. Mater.* **2010**, *12* (5), B179–B183. https://doi.org/10.1002/adem.200980021.

(5)   Prlainovic, N. Z.; Bezbradica, D. I.; Knezevic-Jugovic, Z. D.; Stevanovic, S. I.; Ivic, M. L. A.; Uskokovic, P. S.; Mijin, D. Z. Adsorption of Lipase from Candida Rugosa on Multi Walled Carbon Nanotubes. *J. Ind. Eng. Chem.* **2013**, *19* (1), 279–285. https://doi.org/10.1016/j.jiec.2012.08.012.

(6)   Bencze, L. C.; Bartha-Vari, J. H.; Katona, G.; Tosa, M. I.; Paizs, C.; Irimie, F.-D. Nanobioconjugates of Candida Antarctica Lipase B and Single-Walled Carbon Nanotubes in Biodiesel Production. *Bioresour. Technol.* **2016**, *200*, 853–860. https://doi.org/10.1016/j.biortech.2015.10.072.

(7)   Ke, C.; Li, X.; Huang, S.; Xu, L.; Yan, Y. Enhancing Enzyme Activity and Enantioselectivity of Burkholderia Cepacia Lipase via Immobilization on Modified Multi-Walled Carbon Nanotubes. *RSC Adv.* **2014**, *4* (101), 57810–57818. https://doi.org/10.1039/c4ra10517f.

(8)   Bartha-Vari, J. H.; Tosa, M. I.; Irimie, F.-D.; Weiser, D.; Boros, Z.; Vertessy, B. G.; Paizs, C.; Poppe, L. Immobilization of Phenylalanine Ammonia-Lyase on Single-Walled Carbon Nanotubes for Stereoselective Biotransformations in Batch and Continuous-Flow Modes. *ChemCatChem* **2015**, *7* (7), 1122–1128. https://doi.org/10.1002/cctc.201402894.

(9)   Zaks, A.; Klibanov, A. Enzyme-Catalyzed Processes in Organic-Solvents. *Proc. Natl. Acad. Sci. U. S. A.* **1985**, *82* (10), 3192–3196. https://doi.org/10.1073/pnas.82.10.3192.

(10)   Husson, E.; Humeau, C.; Blanchard, F.; Framboisier, X.; Marc, I.; Chevalot, I. Chemo-Selectivity of the N,O-Enzymatic Acylation in Organic Media and in Ionic Liquids. *J. Mol. Catal. B-Enzym.* **2008**, *55* (3–4), 110–117. https://doi.org/10.1016/j.molcatb.2008.02.004.

(11)   Tufvesson, P.; Annerling, A.; Hatti-Kaul, R.; Adlercreutz, D. Solvent-Free Enzymatic Synthesis of Fatty Alkanolamides. *Biotechnol. Bioeng.* **2007**, *97* (3), 447–453. https://doi.org/10.1002/bit.21258.

(12)   Husson, E.; Humeau, C.; Paris, C.; Vanderesse, R.; Framboisier, X.; Marc, I.; Chevalot, I. Enzymatic Acylation of Polar Dipeptides: Influence of Reaction Media and Molecular Environment of Functional Groups. *Process Biochemistry 44* (4), 428–434.

(13)   Lau, R. M.; van Rantwijk, F.; Seddon, K. R.; Sheldon, R. A. Lipase-Catalyzed Reactions in Ionic Liquids. *Org. Lett.* **2000**, *2* (26), 4189–4191. https://doi.org/10.1021/ol006732d.

(14)   Szelwicka, A.; Boncel, S.; Jurczyk, S.; Chrobok, A. Exceptionally Active and Reusable Nanobiocatalyst Comprising Lipase Non-Covalently Immobilized on Multi-Wall Carbon Nanotubes for the Synthesis of Diester Plasticizers. *Appl. Catal. A-Gen.* **2019**, *574*, 41–47. https://doi.org/10.1016/j.apcata.2019.01.030.

(15)   Raghavendra, T.; Basak, A.; Manocha, L. M.; Shah, A. R.; Madamwar, D. Robust Nanobioconjugates of Candida Antarctica Lipase B - Multiwalled Carbon Nanotubes: Characterization and Application for Multiple Usages in Non-Aqueous Biocatalysis. *Bioresour. Technol.* **2013**, *140*, 103–110. https://doi.org/10.1016/j.biortech.2013.04.071.

(16)   Celia, E. C.; Cernia, E.; D'Acquarica, I.; Palocci, C.; Soro, S. High Yield and Optical Purity in Biocatalysed Acylation of Trans-2-Phenyl-1-Cyclohexanol with Candida Rugosa Lipase in Non-Conventional Media. *J. Mol. Catal. B-Enzym.* **1999**, *6* (5), 495–503. https://doi.org/10.1016/S1381-1177(99)00014-4.

(17)   Palocci, C.; Falconi, M.; Chronopoulou, L.; Cernia, E. Lipase-Catalyzed Regioselective Acylation of Tritylglycosides in Supercritical Carbon Dioxide. *J. Supercrit. Fluids* **2008**, *45* (1), 88–93. https://doi.org/10.1016/j.supflu.2007.11.009.

(18)   Bourkaib, M. C.; Randriamalala, H.; Dettori, L.; Humeau, C.; Delaunay, S.; Chevalot, I.; Guiavarc'h, Y. Enzymatic Synthesis of Geranyl Acetate in Packed Bed Reactor in Supercritical Carbon Dioxide under Various Pressure-Temperature Conditions and Reactor Configurations. *Process Biochem.* **2018**, *71*, 118–126. https://doi.org/10.1016/j.procbio.2018.05.008.

(19)   Kamat, S.; Beckman, E.; Russell, A. Control of Enzyme-Activity by Solvent Engineering in Supercritical Fluids. *Abstr. Pap. Am. Chem. Soc.* **1993**, *205*, 75-BIOT.

(20)   Mercier, G.; Herold, C.; Mareche, J.-F.; Cahen, S.; Gleize, J.; Ghanbaja, J.; Lamura, G.; Bellouard, C.; Vigolo, B. Selective Removal of Metal Impurities from Single Walled Carbon Nanotube Samples. *New J. Chem.* **2013**, *37* (3), 790–795. https://doi.org/10.1039/c2nj41057e.

(21)   Zhang, J.; Zou, H. L.; Qing, Q.; Yang, Y. L.; Li, Q. W.; Liu, Z. F.; Guo, X. Y.; Du, Z. L. Effect of Chemical Oxidation on the Structure of Single-Walled Carbon Nanotubes. *J. Phys. Chem. B* **2003**, *107* (16), 3712–3718. https://doi.org/10.1021/jp027500u.

(22)   Voss, E.; Vigolo, B.; Medjahdi, G.; Herold, C.; Mareche, J.-F.; Ghanbaja, J.; Le Normand, F.; Mamane, V. Covalent Functionalization of Polyhedral Graphitic Particles Synthesized by Arc Discharge from Graphite. *Phys. Chem. Chem. Phys.* **2017**, *19* (7), 5405–5410. https://doi.org/10.1039/c6cp08568g.

(23)   Markiton, M.; Boncel, S.; Janas, D.; Chrobok, A. Highly Active Nanobiocatalyst from Lipase Noncovalently Immobilized on Multiwalled Carbon Nanotubes for Baeyer– Villiger Synthesis of Lactones. *ACS Sustainable Chem. Eng.* **2017**, *5* (2), 1685–1691. https://doi.org/10.1021/acssuschemeng.6b02433.

(24)   Dettori, L.; Jelsch, C.; Guiavarc'h, Y.; Delaunay, S.; Framboisier, X.; Chevalot, I.; Humeau, C. Molecular Rules for Selectivity in Lipase-Catalysed Acylation of Lysine. *Process Biochem.* **2018**, *74*, 50–60. https://doi.org/10.1016/j.procbio.2018.07.021.

(25)   Chiang, I. W.; Brinson, B. E.; Smalley, R. E.; Margrave, J. L.; Hauge, R. H. Purification and Characterization of Single-Wall Carbon Nanotubes. *J. Phys. Chem. B* **2001**, *105* (6), 1157–1161. https://doi.org/10.1021/jp003453z.

(26)   Dyke, C. A.; Tour, J. M. Solvent-Free Functionalization of Carbon Nanotubes. *J. Am. Chem. Soc.* **2003**, *125* (5), 1156–1157. https://doi.org/10.1021/ja0289806.

(27)   Thomy, A.; Duval, X.; Regnier, J. Two-Dimensional Phase Transitions as Displayed by Adsorption Isotherms. *Surf. Sci. Rep.* **1981**, *1* (1), 1–38. https://doi.org/10.1016/0167-5729(81)90004-2.

(28)   Babaa, M. R.; McRae, E.; Delpeux, S.; Ghanbaja, J.; Valsaque, F.; Beguin, F. Surface Characterisation of Template-Synthesised Multi-Walled Carbon Nanotubes. *Chem. Phys. Lett.* **2004**, *396* (1–3), 49–53. https://doi.org/10.1016/j.cplett.2004.07.070.

(29)   Hu, C.-C.; Su, J.-H.; Wen, T.-C. Modification of Multi-Walled Carbon Nanotubes for Electric Double-Layer Capacitors: Tube Opening and Surface Functionalization. *J. Phys. Chem. Solids* **2007**, *68* (12), 2353–2362. https://doi.org/10.1016/j.jpcs.2007.07.002.

(30)   Naseh, M. V.; Khodadadi, A. A.; Mortazavi, Y.; Sahraei, O. A.; Pourfayaz, F.; Sedghi, S. M. Functionalization of Carbon Nanotubes Using Nitric Acid Oxidation and DBD Plasma. **2009**, 3.

(31)   Birch, M. E.; Ruda-Eberenz, T. A.; Chai, M.; Andrews, R.; Hatfield, R. L. Properties That Influence the Specific Surface Areas of Carbon Nanotubes and Nanofibers. *Ann. Occup. Hyg.* **2013**, *57* (9), 1148–1166. https://doi.org/10.1093/annhyg/met042.

(32) Mamane, V.; Mercier, G.; Shukor, J. A.; Gleize, J.; Azizan, A.; Fort, Y.; Vigolo, B. Chemi- vs Physisorption in the Radical Functionalization of Single-Walled Carbon Nanotubes under Microwaves. *Beilstein J. Nanotechnol.* **2014**, *5*, 537–545. https://doi.org/10.3762/bjnano.5.63.

(33) Devaux, X.; Vigolo, B.; McRae, E.; Valsaque, F.; Allali, N.; Mamane, V.; Fort, Y.; Soldatov, A. V.; Dossot, M.; Tsareva, S. Y. Covalent Functionalization of HiPco Single-Walled Carbon Nanotubes: Differences in the Oxidizing Action of H2SO4 and HNO3 during a Soft Oxidation Process. *ChemPhysChem* **2015**, *16* (12), 2692–2701. https://doi.org/10.1002/cphc.201500248.

(34) Hirsch, A. Functionalization of Single-Walled Carbon Nanotubes. *Angew. Chem.-Int. Edit.* **2002**, *41* (11), 1853–1859. https://doi.org/10.1002/1521-3773(20020603)41:11<1853::AID-ANIE1853>3.0.CO;2-N.

(35) dos Santos, P.; Zabot, G. L.; Meireles, M. A. A.; Mazutti, M. A.; Martinez, J. Synthesis of Eugenyl Acetate by,Enzymatic Reactions in Supercritical Carbon Dioxide. *Biochem. Eng. J.* **2016**, *114*, 1–9. https://doi.org/10.1016/j.bej.2016.06.018.

(36) Chrastil, J. Solubility of Solids and Liquids in Supercritical Gases. *J. Phys. Chem.* **1982**, *86* (15), 3016–3021. https://doi.org/10.1021/j100212a041.

(37) Bastida, A.; Sabuquillo, P.; Armisen, P.; Fernandez-Lafuente, R.; Huguet, J.; Guisan, J. M. Single Step Purification, Immobilization, and Hyperactivation of Lipases via Interfacial Adsorption on Strongly Hydrophobic Supports. *Biotechnol. Bioeng.* **1998**, *58* (5), 486–493. https://doi.org/10.1002/(SICI)1097-0290(19980605)58:5<486::AID-BIT4>3.0.CO;2-9.

(38) Reichardt, C.; Utgenannt, S.; Stahmann, K.-P.; Klepel, O.; Barig, S. Highly Stable Adsorptive and Covalent Immobilization of Thermomyces Lanuginosus Lipase on Tailor-Made Porous Carbon Material. *Biochem. Eng. J.* **2018**, *138*, 63–73. https://doi.org/10.1016/j.bej.2018.07.003.

(39) Menaa, B.; Herrero, M.; Rives, V.; Lavrenko, M.; Eggers, D. K. Favourable Influence of Hydrophobic Surfaces on Protein Structure in Porous Organically-Modified Silica Glasses. *Biomaterials* **2008**, *29* (18), 2710–2718. https://doi.org/10.1016/j.biomaterials.2008.02.026.

(40) Barig, S.; Funke, A.; Merseburg, A.; Schnitzlein, K.; Stahmann, K.-P. Dry Entrapment of Enzymes by Epoxy or Polyester Resins Hardened on Different Solid Supports. *Enzyme and Microbial Technology* **2014**, *60*, 47–55. https://doi.org/10.1016/j.enzmictec.2014.03.013.

(41) Plou, F. J.; Cruces, M. A.; Ferrer, M.; Fuentes, G.; Pastor, E.; Bernabe, M.; Christensen, M.; Comelles, F.; Parra, J. L.; Ballesteros, A. Enzymatic Acylation of Di- and Trisaccharides with Fatty Acids: Choosing the Appropriate Enzyme, Support and Solvent. *J. Biotechnol.* **2002**, *96* (1), 55–66. https://doi.org/10.1016/S0168-1656(02)00037-8.

(42) Silveira, E. A.; Moreno-Perez, S.; Basso, A.; Serban, S.; Pestana-Mamede, R.; Tardioli, P. W.; Farinas, C. S.; Castejon, N.; Fernandez-Lorente, G.; Rocha-Martin, J.; et al. Biocatalyst Engineering of Thermomyces Lanuginosus Lipase Adsorbed on Hydrophobic Supports: Modulation of Enzyme Properties for Ethanolysis of Oil in Solvent-Free Systems. *J. Biotechnol.* **2019**, *289*, 126–134. https://doi.org/10.1016/j.jbiotec.2018.11.014.

Supporting Information

Non-covalent and covalent immobilization of *Candida antarctica* Lipase B on chemically modified multiwalled carbon nanotubes for a green acylation process in supercritical CO$_2$

Figure S1 shows mass spectrometry curves of m/z 28 (CO) and m/z 44 (CO$_2$) of fMWCNT; CO and CO$_2$ being the expected fragments for carboxylic group release [1].
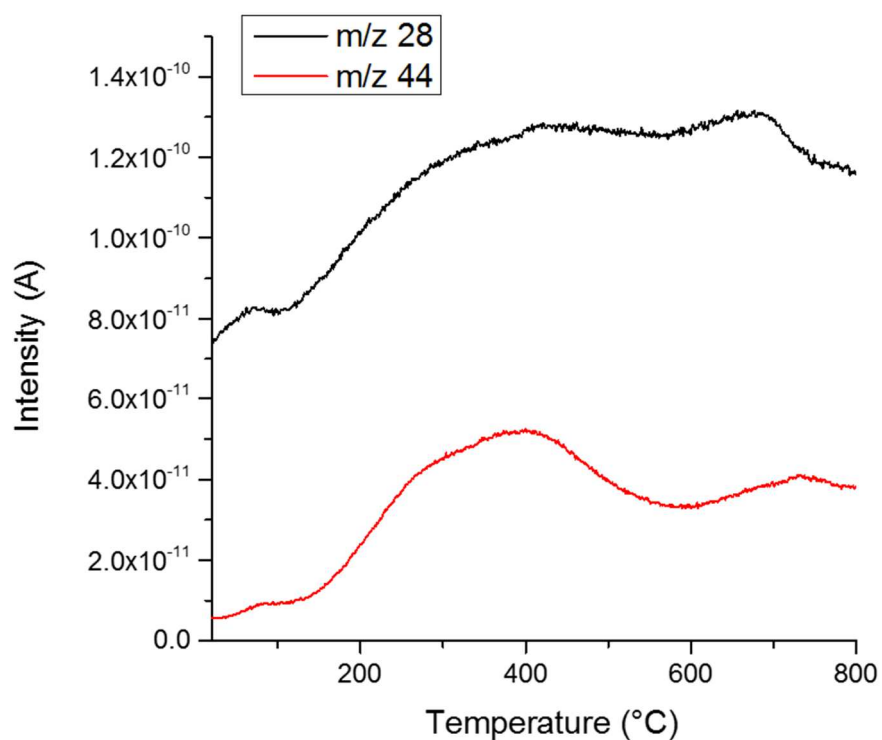

Figure S1 MS curves of CO (m/z 28) and CO$_2$ (m/z 44) during functional group detachment as a function of temperature.

Figure S2 shows the immobilization kinetic for non-covalent adsorption of CalB on functionalized MWCNTs (fMWCNT) from UV-Vis absorption experiments.
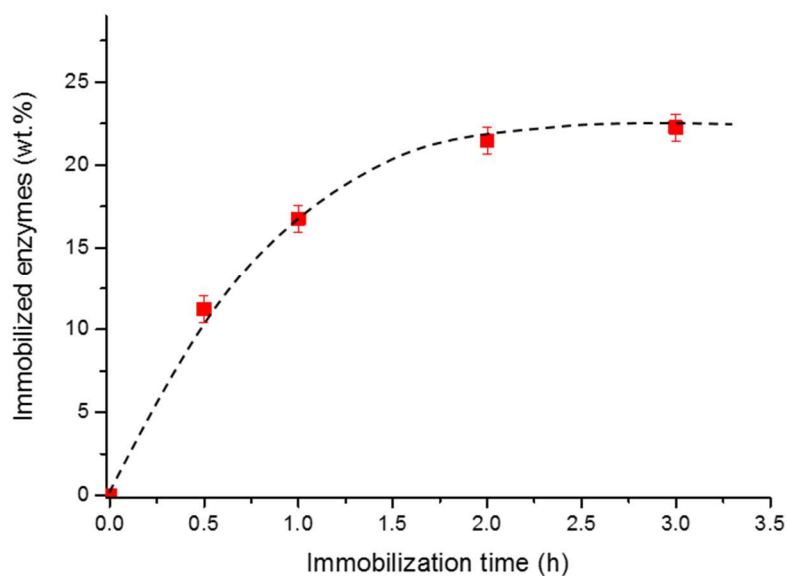
Figure S2 Immobilization kinetic for non-covalent adsorption of CAL-B on fMWCNT from UV-Vis absorption.

Figure S3 shows the m/z corresponding to the expected fragments for phenyl groups, i.e. m/z 50, 51 and 52 for the functionalized MWCNTs (fMWCNT) and MWCNTs where CAL-B was non-covalently immobilized (ncCAL-B@MWCNT). Similar features were obtained for cCAL-B@MWCNT.
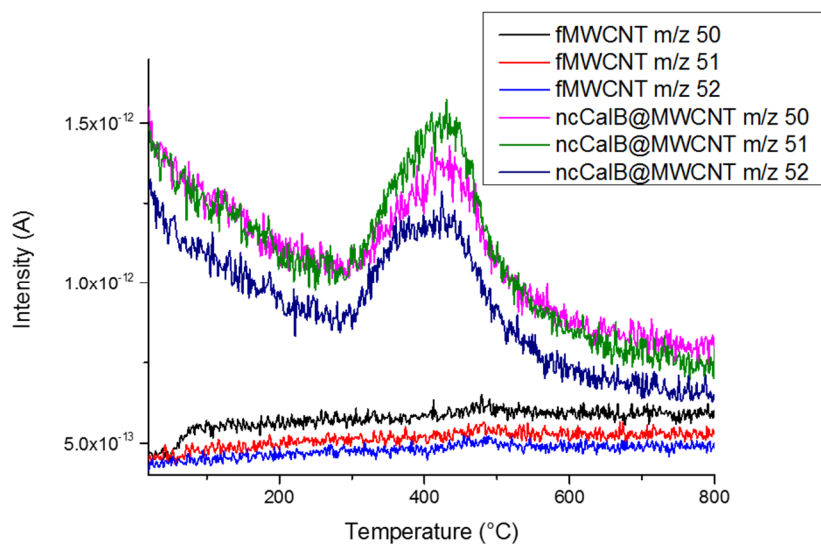
Figure S3 Mass spectrometry fragments for phenyl goups (m/z 50, 51 and 52) of fMWCNT and ncCAL-B@MWCNT.

Table S1 Comparison of apparent Turn Over Frequencies (TOF) expressed in min^{-1} achieved in various publications where esterification reactions were run with the same lipase (*Candida antarctica lipase B, named CAL-B*) immobilized on MWCNTs and using various alcohol/carboxylic acid combinations as substrates.

Immobilization mode	Substrates	Solvent	apparent TOF (min^{-1})	Reactor type	Reference
Covalent	Pentanol / valeric acid	cyclohexane	47.6 with EDAC$^{¥}$	Batch	Raghavendra et al. (2013) [2]

			37.5 with APTES[ϕ]		
Adsorption	n-butanol/ caprylic acid	hexane	33.47	Batch	Pavlidis et al. (2010) [3]
Adsorption	n-butanol / succinic acid	cyclohexane	10.9	Batch	Szelwicka et al. (2019) [4]
Covalent	Geraniol / acetic acid	Supercritical CO_2	$(11.5)/4.1^{§}$	Continuous (PBR)	this study

[¥] EDAC: N-(3-dimethylaminopropyl)-N'-ethylcarbodiimide hydrochloride used as cross-linker

[ϕ] APTES: (3-Aminopropyl)triethoxysilane used as cross-linker

[§] Lower and stabilized apparent TOF (after 1 and 5 cycles) as compared to Raghavendra et al. (covalent binding) or Pavlidis et al., Szelwicka et al. (adsorption). But, in the present study, no organic solvent was used and continuous process instead of batch process was carried out. Another advantage is that water produced is therefore continuously removed from the reactor because slightly soluble in supercritical CO_2 and, consequently, cannot generate reverse hydrolytic reaction (see Bourkaib et al. 2018). Our continuous process is compatible with steady-state esters productions, which is not possible with batch reactors due to water accumulation. The use of one long cycle without depressurization may certainly have allowed to maintain a TOF equal to or slightly below 11.5 min $^{-1}$, pretty close from the one achieved by Szelwicka et al. (2019). Finally, water is also not soluble with the product, geranyl acetate making separation easy.

Detailed explanation regarding water solubility in supercritical CO_2 and why water produced during the esterification did not accumulate in our continuous reactor, thus avoiding the reverse hydrolysis reaction:

Esterification process generates water as a by-product and it is clear that water accumulation may lead to the reverse hydrolytic reaction. In general, when batch reactors are used with organic solvents, water is captured by molecular sieves in the reaction mixture itself. And when

the acyl donor is used as a solvent, the water can be removed by distillation (Tufvesson *et al.* [11]) as a solvent and use of a continuous reactor. The water is removed continuously by the CO_2 during the reaction. Water, despite its polarity, remains slightly soluble in supercritical CO_2. Its solubility in $scCO_2$ has even been quite accurately investigated and modelled, based on experimental data, by Chrastil in 1982. This equation, whose validity has been confirmed by many other papers, is:

$$s = \rho^k \cdot exp^{\left(\frac{a}{T}+b\right)}$$

With s the solubility in $scCO_2$ expressed in g/L, ρ the density of CO_2 in g/L (calculated from T and P), T, the temperature in Kelvin (K), and finally k, a and b as coefficients obtained from non linear regression and identified by Chrastil as:

k=1.549

a=-2826.4

b=-0.807

Applying these values to a supercritical CO_2 at 200 bar and 55°C (328.15 K) with a corresponding density of 754.4 g/L, the solubility is of 2.32 mg/mL of water in $scCO_2$.

In the present work, an equimolar concentration of geraniol and acetic acid of 57 mM/mL of supercritical CO_2 was used at the entrance of the enzymatic packed bed reactor (3 mL/min of $scCO_2$ flow rate). Even assuming a 100 % conversion, 57 mM water/mL of CO_2 would be obtained, that corresponds to only 1.026 mg of water/mL of CO_2. This concentration (assuming a 100 % conversion which is not our case) is about 50 % of the max solubility of water in our $scCO_2$ at 200 bar and 55°C. Therefore there should be no liquid water in the reactor and the slight amount of water is continuously removed from the reactor with $scCO_2$, geranyl acetate and unreacted substrates.

References

[1] Figueiredo, J. L.; Pereira, M. F. R.; Freitas, M. M. A.; Orfao, J. J. M. Modification of the Surface Chemistry of Activated Carbons. *Carbon* **1999**, *37* (9), 1379–1389. https://doi.org/10.1016/S0008-6223(98)00333-9.

[2] Raghavendra, T.; Basak, A.; Manocha, L. M.; Shah, A. R.; Madamwar, D. Robust Nanobioconjugates of Candida Antarctica Lipase B - Multiwalled Carbon Nanotubes: Characterization and Application for Multiple Usages in Non-Aqueous Biocatalysis. *Bioresour. Technol.* **2013**, *140*, 103–110. https://doi.org/10.1016/j.biortech.2013.04.071.

 [3] Pavlidis, I. V.; Tsoufis, T.; Enotiadis, A.; Gournis, D.; Stamatis, H. Functionalized Multi-Wall Carbon Nanotubes for Lipase Immobilization. *Adv. Eng. Mater.* **2010**, *12* (5), B179–B183. https://doi.org/10.1002/adem.200980021.

[4] Szelwicka, A.; Boncel, S.; Jurczyk, S.; Chrobok, A. Exceptionally Active and Reusable Nanobiocatalyst Comprising Lipase Non-Covalently Immobilized on Multi-Wall Carbon Nanotubes for the Synthesis of Diester Plasticizers. *Appl. Catal. A-Gen.* **2019**, *574*, 41–47. https://doi.org/10.1016/j.apcata.2019.01.030.

[5] Tufvesson, P.; Annerling, A.; Hatti-Kaul, R.; Adlercreutz, D. Solvent-Free Enzymatic Synthesis of Fatty Alkanolamides. *Biotechnol. Bioeng.* **2007**, *97* (3), 447–453. https://doi.org/10.1002/bit.21258.